Journal of Magnetic Resonance 212 (2011) 362–369

Contents lists available at SciVerse ScienceDirect

Journal of Magnetic Resonance

journal homepage: www.elsevier.com/locate/jmr

Overcoming apparent Susceptibility-Induced Anisotropy (aSIA) by bipolar double-Pulsed-Field-Gradient NMR

Noam Shemesh, Yoram Cohen *

School of Chemistry, The Raymond and Beverly Sackler Faculty of Exact Sciences, Tel Aviv University, Ramat Aviv, 69978 Tel Aviv, Israel

ARTICLE INFO

Article history:
Received 7 June 2011
Revised 15 July 2011
Available online 29 July 2011

Keywords:
Anisotropy
Diffusion NMR
Mesoporous materials
NMR spectroscopy
Pore morphology
Susceptibility

ABSTRACT

Double-Pulsed-Field-Gradient (d-PFG) MR is emerging as a powerful new means for obtaining unique microstructural information in opaque porous systems that cannot be obtained by conventional single-PFG (s-PFG) methods. The angular d-PFG MR methodology is particularly important since it can utilize the effects of microscopic anisotropy (μA) and compartment shape anisotropy (csA) in the $E(\psi)$ profile at the different t_m regimes to provide detailed information on compartment size and eccentricity. An underlying assumption is that the PFGs that are imparted to weigh diffusion are the only gradients present; however, in realistic systems and especially where there are randomly oriented anisotropic pores, susceptibility effects may induce strong internal gradients. In this study, the effects of such internal gradients on $E(\psi)$ plots obtained from angular d-PFG MR and on microstructural information that can be obtained from s-PFG and d-PFG MR were investigated. First, it was found that internal gradients induce a bias in the s-PFG MR results, thus creating an anisotropy that is not related to microstructure, termed apparent-Susceptibility-Induced-Anisotropy (aSIA). We then show that aSIA effects are also manifest in different ways in the angular d-PFG MR experiment in controlled phantoms and in realistic systems such as quartz sand, emulsions, and biological systems. The effects of aSIA in some cases completely masked the effects of μA and csA; however, we subsequently show that by introducing bipolar gradients to the d-PFG MR (bp-d-PFG), the effects of aSIA can be largely suppressed, restoring the $E(\psi)$ plots that are expected from the theory along with the microstructural information that it conveys. We conclude that when specimens are characterized by strong internal gradients, the novel information on μA and csA that is manifest in the $E(\psi)$ plots can indeed be inferred when bp-d-PFG MR is used, i.e. when bipolar gradients are applied.

1. Introduction

The single-Pulsed-Field-Gradients (s-PFG) diffusion MR methodology (Fig. 1A) [1] offers information on molecular properties such as the diffusion coefficient (D_0) of chemical moieties in solution [2] and can even utilize restricted diffusion processes [3] to report on microstructural properties such as pore size and anisotropy in porous systems ranging from chemistry [4] to material sciences [5,6] and rocks [7], and even to biology [8,9] and medicine [10,11]. Compartment sizes can be obtained from measuring the signal decay as a function of the wavevector $\mathbf{q}$ (where $\mathbf{q} = (2\pi)^{-1}\gamma\delta\mathbf{G}$) up to high q-values; in some cases diffusion–diffraction troughs emerge in the signal decay, offering direct and accurate information on compartment size [12]. These diffraction minima disappear however when size distributions are present [13] and the signal then decays monotonously, but appears non-mono-Gaussian [14–16]. This $E(q)$ signal can be Fourier Transformed, and the root mean squared displacement (rmsd) can be obtained from the resulting displacement probability distribution function (PDF) [14–16]. When anisotropic compartments are coherently organized about a certain axis, i.e. when ensemble anisotropy (eA) exists [17], the macroscopic pore anisotropy can be inferred from diffusion tensor analysis, which yields quantitative and rotationally invariant information on the eigenvalues and eigenvectors [18]. However, it is difficult to infer on anisotropy on a microscopic scale when pores are randomly oriented since diffusion directors are averaged along all directions and only isotropic signals are observed [19].

The double-PFG (d-PFG) MR methodology [20–22] (Fig. 2) employs two gradient vectors $\mathbf{G_1}$ and $\mathbf{G_2}$, which have durations δ_1 and δ_2 respectively, and span the diffusion periods Δ_1 and Δ_2, respectively. The timing between the two diffusion periods is termed the mixing time (t_m). Since two gradient vectors exist, one can define the relative angle between them, termed ψ. Initial studies included comparisons of high q-values $E(q)$ measurements in collinear and orthogonal gradient directions in gray matter [23]

* Corresponding author. Address: School of Chemistry, The Sackler Faculty of Exact Sciences, Tel Aviv University, Ramat Aviv, Tel Aviv 69978, Israel. Fax: +972 3 6407469.
E-mail address: ycohen@post.tau.ac.il (Y. Cohen).

1090-7807/$ - see front matter © 2011 Elsevier Inc. All rights reserved.
doi:10.1016/j.jmr.2011.07.015

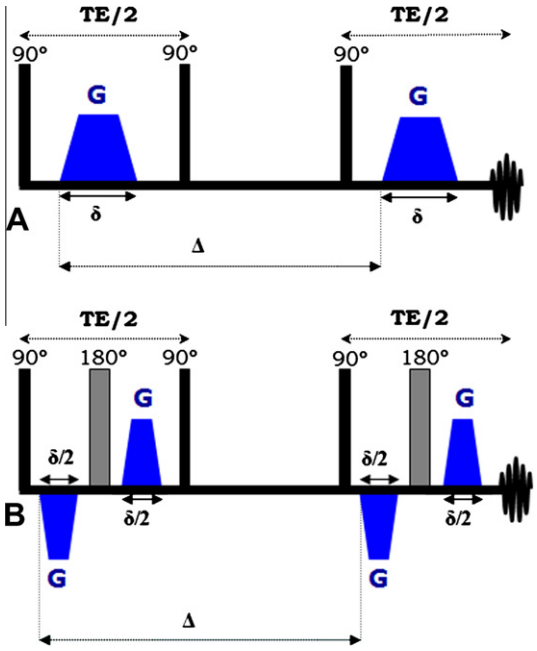

Fig. 1. s-PFG sequences. (A) The single-Stimulated Echo (s-STE) sequence. (B) The bi-polar s-STE (bp-s-STE). Δ – Diffusion period, δ – gradient duration, TE – echo time. Black boxes represent 90° RF pulses, respectively.

and spinal cords [24]. At $\psi = 0°$ and $t_m = 0$ ms, it was later predicted [25] and then experimentally shown [26] that diffusion–diffraction patterns in restricted systems take the form of zero-crossings of the signal decay, which were theoretically predicted [17,25] and then experimentally shown to be robust towards size [13] and orientation [19] distributions. However, such experiments necessitate strong gradients, and furthermore, information on compartment shape is not directly available from the zero-crossings [27].

The angular d-PFG methodology [28] is capable of overcoming some of these drawbacks. In angular d-PFG NMR, the gradient amplitudes are set equal $|\mathbf{G_1}| = |\mathbf{G_2}|$ and only the angle ψ is varied, yielding the so-called angular dependence $E(\psi)$ [17,28–30]. For spherical pores, it was predicted that at short t_m, a bell-shaped $E(\psi)$ profile should emerge, arising from microscopic anisotropy (μA), which directly reports on compartment size even when rather weak gradients are employed [28–30]. Indeed, this has been experimentally observed and validated in controlled systems in spectroscopy [31,32], and, to a certain extent, also in MRI [33–35].

It was later predicted [17] that at short t_m, μA is in fact coupled to yet another parameter termed compartment shape anisotropy (csA), which is in fact related to the local pore eccentricity. Remarkably, it was predicted that at long t_m, μA effects can be decoupled from the effects of csA, thus yielding $E(\psi)$ profiles that are solely dependent on compartment eccentricity, even when pores are completely randomly oriented [17]. At long t_m, a $\cos(2\psi)$-like dependence was predicted for eccentric pores, with increasing amplitude for increasing eccentricity [17], while a ψ-independent profile was predicted for spheres. Indeed, very recently, csA effects were detected for the first time in systems that are not characterized by eA, including controlled porous media [19], emulsions and quartz sand [36], and even isolated gray and white matter of the CNS [37].

Recently, theoretical studies on extension of angular d-PFG NMR to multiple concatenations [38,39], on tensor analysis of the signal to obtain measures of anisotropy that are invariant to rotation [40,41], and on the correlation of the signal with physical interpretation of microstructure [42], as well as monte-carlo simulations of the angular d-PFG MR signal [43] were reported.

In most cases, the applied PFGs are assumed to be the only significant sources of diffusion weighting. However, in many cases, strong internal gradients are additionally present, that are mostly caused by susceptibility effects within the specimen [44–46]. The effect of these internal, or "background" gradients is to add cross-terms to the diffusion NMR signal decay [46]. These cross-terms have been extensively investigated especially in the context of obtaining accurate diffusion coefficients in systems that are characterized by free diffusion [46]. It was shown that the cross-term induced by a temporally constant internal gradient can be effectively suppressed by replacing the PFGs with bipolar PFGs and spacing the π pulses evenly [46,47]. Furthermore, in more complicated scenarios where temporally varying internal gradients exist, methods were suggested to minimize the effects of the cross-terms [48,49]. Other studies in fact utilized the internal field as the only source of gradients, and there it was shown that microstructural information can be inferred from the signal decay due to internal field (DDIF) [7,50].

However, the effects of internal gradients on the microstructural information that can be obtained have not yet been thoroughly studied. One study that investigated diffusion in coherently aligned microcapillaries showed that diffraction troughs that are normally

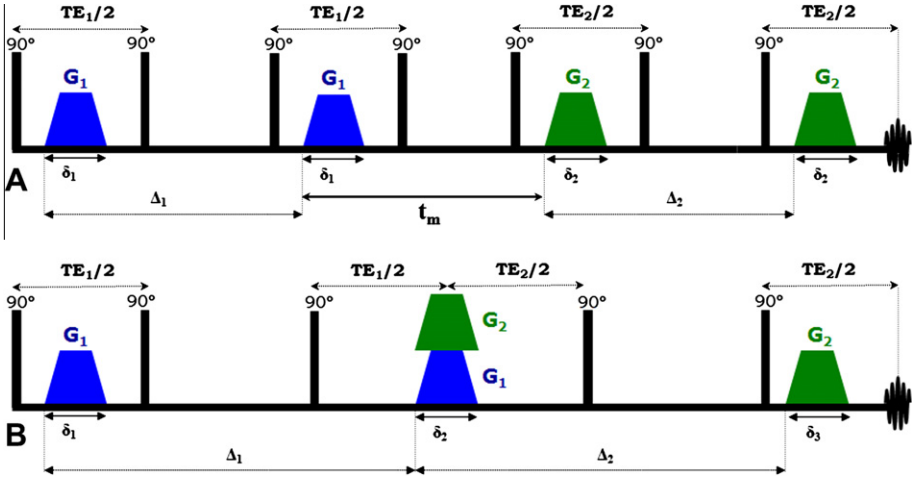

Fig. 2. d-PFG sequences. (A) The double-Stimulated Echo (d-STE) sequence with finite mixing time. (B) The d-STE sequence with zero mixing time. Δ – Diffusion period, δ – gradient duration, TE – echo time, t_m – mixing time. Black and grey boxes represent 90° and 180° RF pulses, respectively. Note that in (A) the case where $\psi = 0°$ is shown, i.e. the gradients in fact encode in the same sense. They graphically appear opposite owing to the two 90° RF pulses in between.

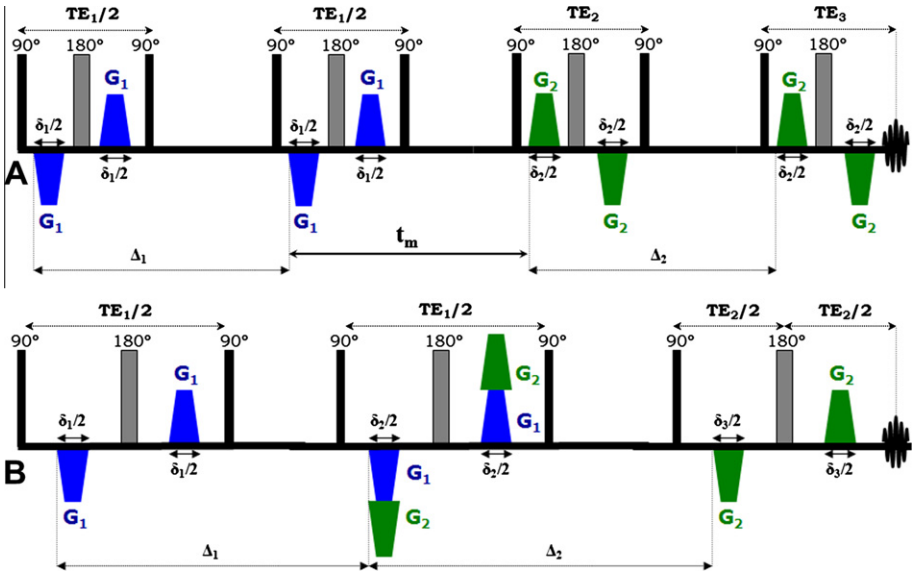

Fig. 3. Bi-polar d-PFG sequences. (A) The bi-polar d-STE (bp-d-STE) sequence with finite mixing time. (B) The bp-d-STE sequence with zero mixing time. Δ – Diffusion period, δ – gradient duration, TE – echo time, t_m – mixing time. Black and grey boxes represent $\pi/2$ and π RF pulses, respectively.

observed and that offer direct microstructural information on pore size [51–53] are lost owing to magnetic inhomogeneity [54]. There, it was also shown that by applying bipolar gradients the diffraction patterns can be fully restored, along with the microstructural information they convey [54]. In another study it was shown that by applying RF gradients (that are robust towards susceptibility related artifacts), a diffraction trough can be restored in inhomogeneous media [55]; in both cases, the microstructural information has been recovered.

The robustness of double-PFG MR to size and orientation distributions, along with its ability to portray compartment shape anisotropy makes it a good candidate for uniquely characterizing many types of porous systems where susceptibility effects may be very significant. However, the effects of internal gradients on the angular dependencies arising from d-PFG have not yet been studied. Here, we study these effects in both controlled systems as well as in several applications such as quartz sand, emulsions, and even biological systems such as yeast cells. We first show that internal gradients can induce an apparent anisotropy in both s- and d-PFG experiments. Subsequently, we show experimentally that bipolar d-PFG NMR (bp-d-PFG) NMR (Fig. 3) can effectively suppress the effects of internal gradients and offer accurate microstructural information in these systems.

2. Materials and methods

2.1. Preparation of the specimens used in this study

The preparation of the controlled porous media was previously described [19]. Briefly, hollow microcapillaries with well defined inner diameter (ID) (PolyMicro Technologies, Phoenix AZ, USA) were manually cut to very small pieces and were filled by water by immersing the particles in distilled water for several days. The resultant porous media was poured into an eight or in some cases 10 mm NMR tube containing Fluorinert (Sigma–Aldrich, Rehovot, Israel).

The sand specimen was prepared simply by packing clean quartz sand into an NMR tube and filling it with distilled water. After the sand was clearly wet, the clear water layer above the sand was aspired using a pipette. The NMR tube containing the sand specimen was then used without any further process.

The yeast cells specimen was prepared as follows: The yeast were hydrated with PBS, then centrifuged for 10 min with 1000 rpm. The yeast were then suspended in paraformaldehyde (Sigma–Aldrich, Rehovot, Israel) fixative for 90 min, then washed twice with Phosphate-Buffer-Saline (PBS) (Sigma–Aldrich, Rehovot, Israel). The cells were centrifuged again for 10 min and 1000 rpm after the second wash, and the supernatant fluid was removed. The yeast cells were then suspended in a small amount of PBS, which was poured to an 8 mm NMR tube. The fixated cells were allowed to settle overnight at 4 °C, and the water that collected above the yeast was again removed prior to the NMR experiments.

2.2. NMR experiments

All experiments were performed on an Bruker 8.4 T NMR spectrometer equipped with a Micro5 probe capable of producing nominal pulsed gradients of up to 1900 mT/m in each direction. The temperature was kept constant throughout the experiments. For a general review on the angular d-PFG methodology, see [27]. Briefly, all angular experiments were performed using the following methodology: the gradient amplitudes were set constant, i.e. $|\mathbf{G_1}| = |\mathbf{G_2}|$, and $\mathbf{G_1}$ was fixed in the x-direction. The orientation of $\mathbf{G_2}$ was varied in 25 equal steps along 360° in the X–Y plane (perpendicular to the direction of B_0).

To infer on the presence of aSIA effects, both s-PFG and d-PFG experiments were performed first using sequences employing conventional, monopolar gradients (Figs. 1A and 2), and then the experiments were repeated using sequences that replaced the monopolar gradients with bipolar gradients, i.e. bp-s-PFG and angular bp-d-PFG sequences (Figs. 1B and 3). The gradients in monopolar sequences (Figs. 1A and 2) are characterized by their duration δ and their amplitude $|\mathbf{G}|$. To maintain the same q-value in the sequences employing bipolar gradients (Figs. 1B and 3), the gradient amplitude $|\mathbf{G}|$ was kept identical to the monopolar version, but the gradient pulse was split into two lobes having duration $\delta/2$, and a π-pulse was symmetrically placed between the two lobes [46,47], affording the bp-s-PFG or bp-d-PFG sequences shown in Figs. 1B and 3, respectively. For all experiments the TR was set to 4.5 s.

2.3. Experimental parameters for NMR experiments

2.3.1. Randomly oriented pores with ID = 29 ± 1 μm

Single-PFG and bp-s-PFG were conducted with the sequences shown in Fig. 1A and B respectively, with the following parameters: $\Delta/\delta = 250/3$ ms, 9 q-values were collected with G_{max} of 470 mT/m, resulting in a maximum q-value of 766 cm^{-1}. The number of scans (NS) was set to eight. The SNR of the first q-value was ~6500.

2.3.2. Randomly oriented pores with ID = 10 ± 1 μm

To show compartment shape anisotropy, the angular d-PFG experiments were performed as described above, with the monopolar and bipolar sequences shown in Figs. 2A and B and 3A and B, respectively. The following parameters were used for long t_m: $\Delta_1 = \Delta_2 = 250$ ms, $\delta_1 = \delta_2 = 3$ ms and $t_m = 18$ ms. For the short t_m: $\Delta_1 = \Delta_2 = 250$ ms, $\delta_1 = \delta_2 = 3$ ms and $t_m = 0$ ms. The $E(\psi)$ profiles were measured for $2q = 255$ cm^{-1} as well as $2q = 447$ cm^{-1}. The SNR for both q-values was larger than 110 at $\psi = 0°$ for both monopolar and bipolar angular d-PFG experiments. The NS was set to 32.

2.3.3. Quartz sand experiments

Comparison between conventional and bipolar d-PFG was performed on the fine grains specimen with the following parameters: The angular d-PFG experiments were performed as described previously, with the monopolar and bipolar sequences shown in Figs. 2B and 3B, respectively. The following parameters were used: $\Delta_1 = \Delta_2 = 50$ ms, $\delta_1 = \delta_2 = \delta_3 = 3$ ms and $t_m = 0$ ms. The measurements were performed at $2q = 631$ cm^{-1}, and the SNR at $\psi = 0°$ was larger than 150 for both monopolar and bipolar d-PFG experiments. The NS was set to 24.

2.3.4. Yeast cells

The monopolar and bipolar angular d-PFG experiments were performed with the sequences shown in Figs. 2B and 3B, respectively with the following parameters $\Delta_1 = \Delta_2 = 200$ ms, $\delta_1 = \delta_2 = 3$ ms and $t_m = 0$ ms. The $E(\psi = 180°)$ value for the monopolar experiment was replaced with the average of the two neighboring points owing to a signal fluctuation. The measurements were performed up to $2q = 2043$ cm^{-1}, and the SNR at $\psi = 0°$ was larger than 200 for both monopolar and bipolar d-PFG experiments at $2q = 2043$ cm^{-1}. The NS was set to eight.

2.3.5. Experiments on the emulsion

system. The angular d-PFG and bp-d-PFG experiments were performed with the sequences shown in Figs. 2B and 3B, respectively. The following parameters were used: $\Delta_1 = \Delta_2 = 200$ ms, $\delta_1 = \delta_2 = \delta_3 = 3$ ms and $t_m = 0$ ms. The $E(\psi)$ profiles were measured for $2q = 283$ cm^{-1} as well as $2q = 1604$ cm^{-1}. The NS was set to eight. The SNR at $2q = 283$ cm^{-1} and $\psi = 0°$ was larger than 1000 for both monopolar and bipolar angular d-PFG experiments while the SNR at $2q = 1604$ cm^{-1} and $\psi = 0°$ was larger than 15 for both monopolar and bipolar angular d-PFG experiments.

3. Results and discussion

Fig. 4A shows s-PFG NMR experiments conducted on a controlled specimen that has cylindrical pores that are completely randomly oriented using the sequence shown in Fig. 1A. As could be expected, the line width in this specimen is very large, ~0.5 kHz, manifesting the large susceptibility differences arising from all the cylinders that are not parallel to the magnetic field B_0. Surprisingly, Fig. 4A shows anisotropy in the NMR signal decay, with diffusion in the z-direction slower compared to diffusion in the x- and y-directions, which appear very similar. The ground truth in this specimen is well known, and the experimental results disagree profoundly with diffusion in randomly oriented cylindrical compartments, which should manifest isotropic diffusion in the s-PFG MR experiment. The experimental results shown in Fig. 4A could be consistent in fact only with coherently organized oblate compartments, where diffusion in the z-direction is expected to appear slower than diffusion in the x- and y-directions. Fig. 4B shows bp-s-PFG NMR experiments conducted on the same phantom with identical diffusion weighting but with the sequence shown in Fig. 1B. Here, isotropic signal decay is clearly observed. Moreover, the signal decay itself is different and decays more rapidly compared to the signal decay observed in monopolar s-PFG MR experiments. As explained above, the isotropic signal decay is expected since s-PFG MR can only detect eA, which is not present in this specimen. Therefore, the anisotropy that is observed in the s-PFG NMR experiments is in fact induced by susceptibility effects, as clearly shown from the suppression of this anisotropy by the bp-s-PFG NMR. Since experiments employing monopolar gradients show anisotropy that is "apparent" but does not reflect the actual geometry of the investigated system, and the apparent anisotropy appears to be merely induced by background gradients, we term this anisotropy "apparent-Susceptibility-Induced-Anisotropy" (aSIA).

At $t_m = 0$ ms, the $E(\psi)$ angular dependencies arising from angular d-PFG NMR experiments in randomly oriented anisotropic compartments were predicted [17] and then experimentally shown [19] to follow a modulated bell shaped curve. This behavior is a manifestation of both μA and csA on the $E(\psi)$ dependence, from which the compartment size and its eccentricity can in principle be extracted. To investigate how the effects of aSIA influence angular d-PFG NMR measurements, we performed angular d-PFG

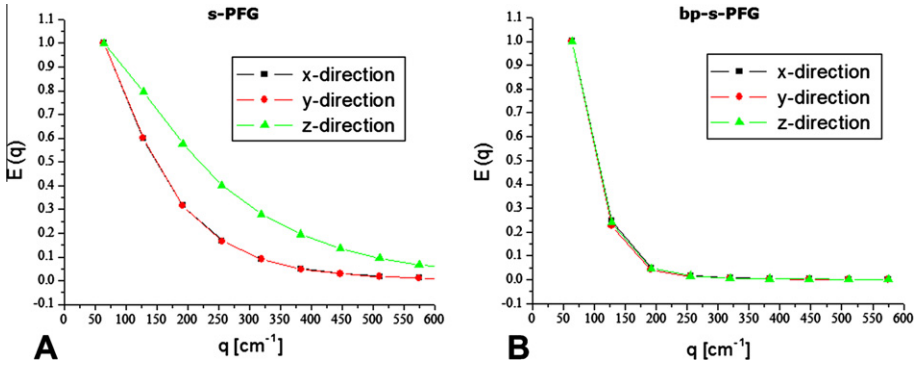

Fig. 4. s-PFG NMR experiments on randomly oriented locally cylindrical pores with ID = 29 ± 1 μm. (A) monopolar s-PFG NMR and (B) bp-s-PFG NMR. Note that the signal decays at different rates when s-PFG is used, leading to erroneous interpretation of pore shape due to aSIA effects. The bp-s-PFG NMR corrects these effects, and yields the accurate isotropic decay.

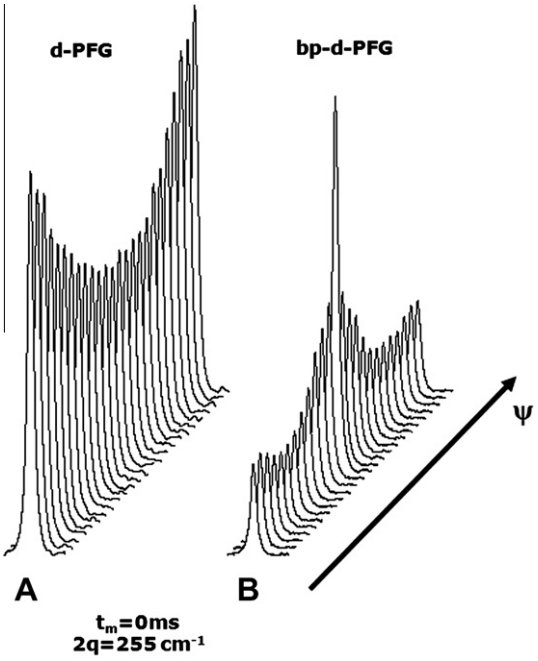

Fig. 5. Stackplot of angular d-PFG NMR experiments on randomly oriented locally cylindrical pores with ID = 10 ± 1 μm. (A) Angular d-PFG NMR note that here, bipolar gradients are used. (B) Angular bp-d-PFG NMR (note that here, bipolar gradients are used). An inverted angular dependence is observed when monopolar gradients are used. Application of bipolar gradients produces the expected angular dependence, from which accurate morphological features can be extracted.

and angular bp-d-PFG NMR experiments on the same phantom where the linewidth was about 0.5 kHz. Fig. 5 shows a stackplot of the NMR signal from these experiments at $2q = 255\ \mathrm{cm}^{-1}$ and at $t_m = 0$ ms. Remarkably, and completely contrary to the theoretical predictions, Fig. 5A shows that $E(\psi)$ *decreases* up to $\psi = 180°$, and then increases back to its original value at $\psi = 360°$. The signal decreases by more than a factor of 2 at $\psi \sim 180°$. These observations are clearly inconsistent with the expected $E(\psi)$ profile in such specimens; in randomly oriented cylinders, $E(\psi)$ should be governed by μA, which gives rise to bell shaped dependencies, and by csA, which modulates these $E(\psi)$ curves. Therefore, a modulated bell-shaped curve is expected [17]. The observed $E(\psi)$ dependence from angular d-PFG MR in this system (Fig. 5A) in fact does not seem to represent the manifestations of neither of these important microstructural parameters; rather, it seems that the effects of μA and csA are being masked by the effects of aSIA. This can be ascertained when the same experiments are performed but this time with a sequence employing bipolar gradients (bp-d-PFG) (Fig. 5B). Indeed, when angular bp-d-PFG NMR experiments were performed, the $E(\psi)$ signal returned to its expected form, showing a modulated bell shaped dependence. Here, the signal decreased only up to $\psi \sim 90°$, and then increased gradually up to $\psi = 180°$; this behavior was mirrored subsequently up to $\psi = 360°$. These modulated curves indeed represent the μA and csA present in the specimen, from which the compartment size and eccentricity can be accurately extracted [17,19]. Therefore, it seems that the effects of aSIA, which masked the effects of μA and csA in the $E(\psi)$ profile of angular d-PFG NMR experiments, is sufficiently suppressed.

Fig. 6 shows angular d-PFG and bp-d-PFG experiments at both short and long mixing times in a phantom where cylindrical compartments having ID = 10 μm that were randomly oriented (the line width was again on the order of ~0.5 kHz). The effects of aSIA are clear in all conventional angular d-PFG NMR experiments, at both mixing times, and at both q-values shown (Fig. 6A and C). When monopolar gradients are used, the $E(\psi)$ plots appear inverted, and do not represent the effects of μA and csA on the angular dependence. The inverted dependencies therefore cannot be used to extract meaningful microstructural information from the specimen. Importantly, it is impossible to infer on the presence of csA, which reflects the eccentricity of the pores present in the specimen; such unique information is one of the main advantages of angular d-PFG NMR, since it inherently cannot be obtained from s-PFG MR approaches. Therefore, the loss of this information owing to aSIA represents a major drawback for the angular d-PFG methodology in such specimens.

By contrast, for both t_m regimes, when the bp-d-PFG NMR is performed, the application of bipolar gradients seems to alleviate the aSIA effects substantially, and the modulated angular dependence appears in the $E(\psi)$ plots (Fig. 6B and D). In a recent study it was shown that indeed, these $E(\psi)$ dependencies can be in fact used to extract compartment size, and importantly, to infer on the presence of compartment shape anisotropy from the short and long t_m regime, respectively. This information was completely unavailable from s-PFG MR [19]. Indeed, in such scenarios where compartments are randomly oriented, information on the underlying compartment eccentricity can be uniquely obtained from angular d-PFG NMR at long t_m; however, the results shown in Fig. 6 clearly demonstrate that bipolar gradients are imperative for one to obtain a meaningful $E(\psi)$ profile. Indeed, the data from conventional d-PFG MR experiments was so distorted and the inverted angular dependence was so different compared to the expected modulated $E(\psi)$ curves, that attempting to fit such data to the theory seems problematic, and accurate compartment sizes could not be obtained.

After observing the effects of aSIA in controlled phantoms, we sought to investigate aSIA effects in more realistic specimens that were recently characterized uniquely by angular bp-d-PFG NMR [36]. We therefore conducted and compared angular d-PFG and bp-d-PFG experiments in three different specimens: water diffusing between quartz sand grains, the oil component of an oil-in-water emulsion, and finally, a biological specimen, namely fixed yeast cells. Fig. 7 shows the results of these experiments.

The line width of a pulse-acquire NMR experiment in the sand specimen was ~1.2 kHz, manifesting very large internal gradients within the sand. Indeed, when the conventional angular d-PFG NMR experiments were performed, the inverted angular dependence was clearly observed, showing the masking of aSIA effects on the $E(\psi)$ profile, and the masking of the effects of μA and csA on the $E(\psi)$ profiles (Fig. 7A). However, when the angular bp-d-PFG NMR experiments were performed, the inverted angular dependence disappeared, giving rise to a pronounced, bell-shaped $E(\psi)$ profile, from which meaningful information could be obtained [36].

In the fixed yeast cells, the line width was much smaller, ~30 Hz, and we therefore expected aSIA effects to be much less pronounced. Indeed, the effects of aSIA were not apparent at the low q-values; however, a different form of aSIA was observed at higher q-values. Here, the angular dependence does not appear inverted; rather, we observed a plateau-like feature in the $E(\psi)$ angular dependence in monopolar angular d-PFG experiments. The plateau-like behavior was observed around $\psi \sim 180 \pm 90°$ (Fig. 7B), and was also observed in other biological specimens such as fixed optic nerves (data not shown). Note that the signal is not exactly a plateau, and there is a slight decrease around $\psi \sim 180 \pm 30°$. When angular bp-d-PFG NMR experiments were performed however, these effects seem to be largely suppressed, and the expected bell shaped $E(\psi)$ profile is observed. It should be noted that under light microscopy, the cells appear spherical, and therefore a smooth bell shaped curve is expected by the theory for spherical compartments. Indeed, in a recent study, the angular

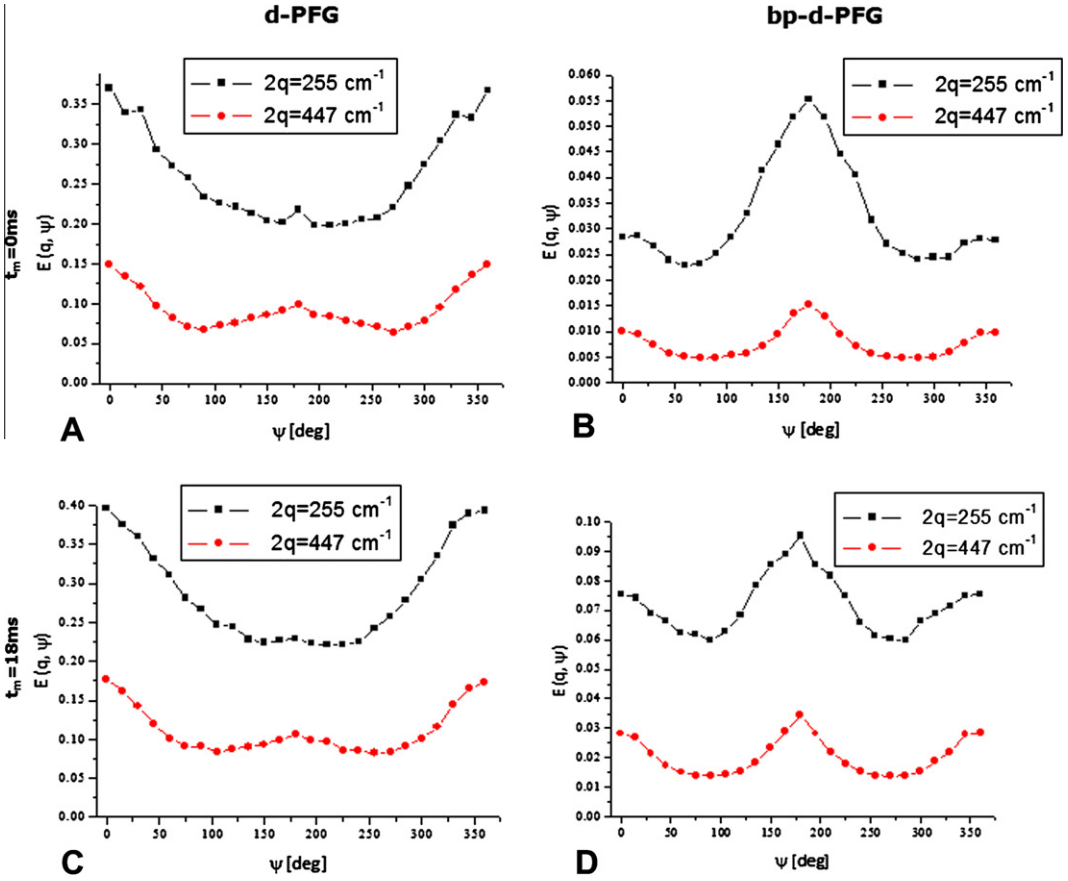

Fig. 6. Angular d-PFG NMR experiments on randomly oriented locally cylindrical pores with ID = 10 ± 1 μm. (A) Angular d-PFG NMR with monopolar gradients (t_m = 0 ms). (B) Angular bp-d-PFG NMR with bipolar gradients (t_m = 0 ms). (C) Angular d-PFG NMR with monopolar gradients (t_m = 18 ms). (D) Angular bp-d-PFG NMR with bipolar gradients conducted (t_m = 18 ms).

bp-d-PFG NMR showed that the cells are in fact spherical from a ψ-independent profile at long t_m [36]. Here, the bipolar gradients indeed appear to correct the plateau-like effects at short t_m, and therefore it can be inferred that this is a different, more subtle effect of aSIA, that is manifested only at higher q-values when the susceptibility effects are not severe.

In the toluene-in-water emulsion, the line width of the methyl peak of toluene in a pulse-acquire NMR experiment was comparable to that of the yeast cells, and the line width was ~30 Hz. Here, at low q-values, both d-PFG and bp-d-PFG angular experiments provide very similar information, both showing a bell-shaped $E(\psi)$ profile (Fig. 7C). However, as the q-values are increased, again, the effect of aSIA now does not appear as a plateau, but as a symmetrical decrease of the signal around $\psi \sim 180 \pm 90°$. It may be that this is the same effect as was found in the yeast cells, only more pronounced in the emulsion. Again, it can be shown that this is an aSIA effect, since it is suppressed when angular bp-d-PFG NMR is used. In the angular bp-d-PFG MR experiments, the expected form is restored in the $E(\psi)$ plots, i.e. a modulated bell-shaped curve is in fact observed that manifests the effects of μA and csA.

Komlosh et al. investigated the $E(q)$ signal decay at long t_m in different collinear and orthogonal d-PGSE experiments in a "gray matter phantom", which consisted of water filled capillaries having a random orientation [23]. There, it was clearly observed that the signal decreased from the X_X direction (which corresponds to $\psi = 0°$) to the X_Y direction (which corresponds to $\psi = 90°$), and then a further decrease was shown between X_X and X_-X (which corresponds to $\psi = 180°$), and it was tentatively suggested that these effects may be due to susceptibility, although other mechanisms were proposed as well. The effects observed in [23] are consistent with what was observed in the full $E(\psi)$ profile in this study (Fig. 5A), and can now be explained as an aSIA effect, especially since the predicted [17] angular dependence was restored by applying bipolar gradients. Another experimental angular d-PFG study was recently conducted by Koch and Finsterbusch using an imaging sequence on water diffusing between packed acrylate beads, pig spinal cords, and radish [33]. In some of their data, inverted angular dependencies can also be seen, that are likely effects of aSIA on the $E(\psi)$ profiles.

Another previous study showed that the highly informative diffusion–diffraction troughs that can be observed in s-PFG MR of monodisperse compartments are in fact lost in the presence of strong field inhomogeneity and are recovered once bp-s-PFG MR is applied [54]. Recently, it was shown that when pores are randomly oriented, the diffraction patterns are lost in bp-s-PFG MR, but are recovered in bp-d-PFG MR since the diffraction patterns originate from zero-crossing of the signal [19]. We note that there, monopolar d-PFG MR did not exhibit zero-crossings, again owing to aSIA effects, that were successfully suppressed when bipolar-d-PFG MR was performed [19].

The effects of background gradients are usually analyzed in terms of the effective gradient amplitudes in $E(q)$ profiles [46], leading to the cross-terms between diffusion and background gradients. Here, the interaction of the background gradient with the d-PFG MR gradients was shown at constant q-values, probably emphasizing an angular dependence of the cross-terms. Further theoretical studies examining the effect of background gradients on the angular d-PFG MR will be needed to decipher the exact origin of the inverted curves observed here.

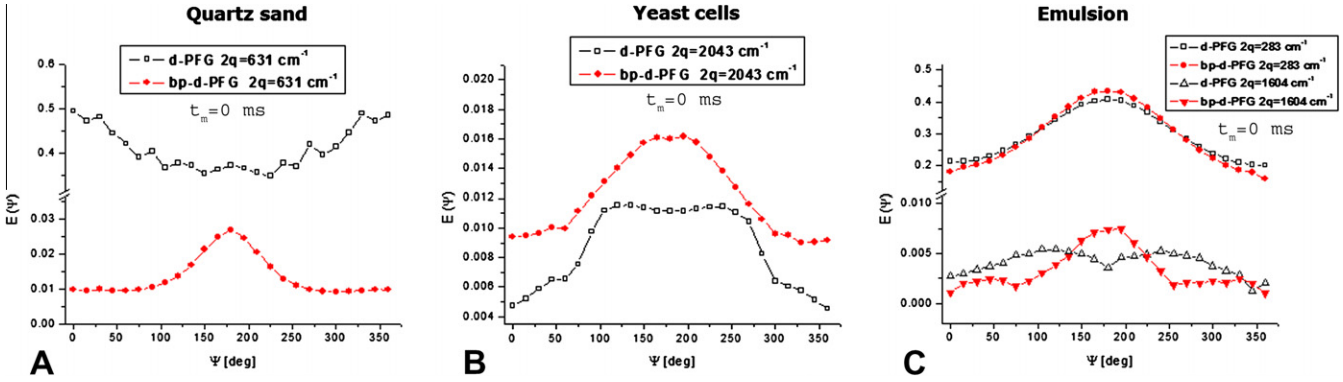

Fig. 7. Effects of aSIA on $E(\psi)$ profiles at $t_m = 0$ ms in realistic specimens using conventional angular d-PFG and bp-d-PFG NMR. (A) Specimen consisting of fine Quratz sand grains (linewidth – 1.2 kHz). In d-PFG MR (squares), an inverted angular dependence is observed. However, in bp-d-PFG (circles), an angular bell-shaped function appears. (B) Yeast cells (linewidth ~30 Hz). In d-PFG MR (squares), the smooth bell-shaped profile that is expected from spherical compartments is distorted. This distortion was easily corrected using bp-d-PFG (circles). E(ψ = 180°) was replaced with the average of the two neighboring points owing to a signal fluctuation in the conventional d-PFG data. (C) Emulsion system (toluene peak, line width ~30 Hz). The angular dependence at low q-values appears similar between d-PFG (squares) and bp-d-PFG experiments (circles). However, at higher q-values, the angular dependence is distorted in d-PFG experiments (black upper triangles). The bp-d-PFG (red lower triangles) experiments show the expected angular $E(\psi)$ profile.

4. Conclusions

The angular d-PFG methodology is emerging as a means for obtaining novel and unique microstructural information on μA and csA that cannot be obtained from conventional s-PFG MR methods, especially in scenarios where eA is not present. We have shown here that susceptibility effects can lead to anisotropy that is not related to microstructure even in s-PFG MR; we subsequently showed that aSIA is also observed in angular d-PFG NMR, masking the effects of μA and csA and leading to $E(\psi)$ that cannot be interpreted with respect to microstructure. Importantly, we have shown that applying bipolar gradients in the angular bp-d-PFG NMR methodology suppresses the effects of aSIA to a good extent, and the information on the underlying microstructure can be recovered. We conclude that angular bp-d-PFG NMR may indeed become important in characterizing even highly inhomogeneous porous media in different areas of both basic and applied research.

Acknowledgments

Y.C. and N.S. were partially supported by the CONNECT consortium administered by the European commission under Framework Package 7. N.S. would like to gratefully acknowledge the Clore Scholars Program for a scholarship. Y.C. and N.S. would like to thank Prof. Aldo Shemesh from the Weizmann institute of Science for the Quartz sand specimens.

References

[1] E.O. Stejskal, J.E. Tanner, Spin diffusion measurements – spin echoes in presence of a time-dependent field gradient, J. Chem. Phys. 42 (1965) 288–292.
[2] Y. Cohen, L. Avram, L. Frish, Diffusion NMR spectroscopy in supramolecular and combinatorial chemistry: an old parameter – new insights, Angew. Chem. Int. Ed. 44 (2005) 520–554.
[3] D.S. Grebenkov, NMR survey of reflected Brownian motion, Rev. Mod. Phys. 79 (2007) 1077–1137.
[4] J. Karger, D. Michel, Special issue: magnetic resonance of porous materials, Magn. Reson. Chem. 37 (1999) S1–S159.
[5] A.T. Watson, C.T.P. Chang, Characterizing porous media with NMR methods, Prog. Nucl. Magn. Reson. Spectrosc. 31 (1997) 343–386.
[6] R.W. Mair, M.S. Rosen, R. Wang, D.G. Cory, R.L. Walsworth, Diffusion NMR methods applied to xenon gas for materials study, Magn. Reson. Chem. 40 (2002) S29–S39.
[7] Y.Q. Song, S.G. Ryu, P.N. Sen, Determining multiple length scales in rocks, Nature 406 (2000) 178–181.
[8] P.W. Kuchel, A. Coy, P. Stilbs, NMR "diffusion–diffraction" of water revealing alignment of erythrocytes in a magnetic field and their dimensions and membrane transport characteristics, Magn. Reson. Med. 37 (1997) 637–643.
[9] G. Pages, T.W. Yau, P.W. Kuchel, Erythrocyte shape reversion from echinocytes to discocytes: kinetics via fast-measurement NMR diffusion–diffraction, Magn. Reson. Med. 64 (2010) 645–652.
[10] P.J. Basser, J. Mattiello, D. Lebihan, Diffusion tensor spectroscopy and imaging, Biophys. J. 66 (1994) 259–267.
[11] C. Beaulieu, The basis of anisotropic water diffusion in the nervous system – a technical review, NMR Biomed. 15 (2002) 435–455.
[12] P.T. Callaghan, A. Coy, D. Macgowan, K.J. Packer, F.O. Zelaya, Diffraction-like effects in NMR diffusion studies of fluids in porous solids, Nature 351 (1991) 467–469.
[13] N. Shemesh, E. Özarslan, P.J. Basser, Y. Cohen, Detecting diffusion–diffraction patterns in size distribution phantoms using double-pulsed field gradient (d-PFG) NMR: theory and experiments, J. Chem. Phys. 132 (2010) 034703.
[14] P.T. Callaghan, D. Macgowan, K.J. Packer, F.O. Zelaya, High-resolution q-space imaging in porous structures, J. Magn. Reson. 90 (1990) 177–182.
[15] D.G. Cory, A.N. Garroway, Measurement of translational displacement probabilities by NMR – an indicator of compartmentation, Magn. Reson. Med. 14 (1990) 435–444.
[16] Y. Cohen, Y. Assaf, High b-value q-space analyzed diffusion-weighted MRS and MRI in neuronal tissues – a technical review, NMR Biomed. 15 (2002) 516–542.
[17] E. Özarslan, Compartment shape anisotropy (CSA) revealed by double pulsed field gradient MR, J. Magn. Reson. 199 (2009) 56–67.
[18] P.J. Basser, J. Mattiello, D. Lebihan, Estimation of the effective self-diffusion tensor from the NMR spin-echo, J. Magn. Reson. B 103 (1994) 247–254.
[19] N. Shemesh, E. Özarslan, T. Adiri, P.J. Basser, Y. Cohen, Noninvasive bipolar double-pulsed-field-gradient NMR reveals signatures for pore size and shape in randomly oriented, polydisperse, inhomogeneous porous media, J. Chem. Phys. 133 (2010) 044705.
[20] Y. Cheng, D.G. Cory, Multiple scattering by NMR, J. Am. Chem. Soc. 121 (1999) 7935–7936.
[21] D.G. Cory, A.N. Garroway, J.B. Miller, Applications of spin transport as a probe of local geometry, Polymer Preprints 31 (1990) 149–150.
[22] P.T. Callaghan, M.E. Komlosh, Locally anisotropic motion in a macroscopically isotropic system: displacement correlations measured using double pulsed gradient spin-echo NMR, Magn. Reson. Chem. 40 (2002) S15–S19.
[23] M.E. Komlosh, F. Horkay, R.Z. Freldlin, U. Nevo, Y. Assaf, P.J. Basser, Detection of microscopic anisotropy in gray matter and in a novel tissue phantom using double Pulsed Gradient Spin Echo MR, J. Magn. Reson. 189 (2007) 38–45.
[24] M.E. Komlosh, M.J. Lizak, F. Horkay, R.Z. Freidlin, P.J. Basser, Observation of microscopic diffusion anisotropy in the spinal cord using double-pulsed gradient spin echo MRI, Magn Reson. Med. 59 (2008) 803–809.
[25] E. Özarslan, P.J. Basser, MR diffusion–"diffraction" phenomenon in multi-pulse-field-gradient experiments, J. Magn. Reson. 188 (2007) 285–294.
[26] N. Shemesh, Y. Cohen, The effect of experimental parameters on the signal decay in double-PGSE experiments: negative diffractions and enhancement of structural information, J. Magn. Reson. 195 (2008) 153–161.
[27] N. Shemesh, E. Özarslan, M.E. Komlosh, P.J. Basser, Y. Cohen, From single-pulsed field gradient to double-pulsed field gradient MR: gleaning new microstructural information and developing new forms of contrast in MRI, NMR Biomed. 23 (2010) 757–780.
[28] P.P. Mitra, Multiple wave-vector extensions of the NMR Pulsed-Field-Gradient spin-echo diffusion measurement, Phys. Rev. B 51 (1995) 15074–15078.
[29] E. Özarslan, P.J. Basser, Microscopic anisotropy revealed by NMR double pulsed field gradient experiments with arbitrary timing parameters, J. Chem. Phys. 128 (2008) 154511.
[30] E. Özarslan, N. Shemesh, P.J. Basser, A general framework to quantify the effect of restricted diffusion on the NMR signal with applications to double pulsed field gradient NMR experiments, J. Chem. Phys. 130 (2009) 104702.

[31] N. Shemesh, E. Özarslan, P.J. Basser, Y. Cohen, Measuring small compartmental dimensions with low-q angular double-PGSE NMR: the effect of experimental parameters on signal decay, J. Magn. Reson. 198 (2009) 15–23.
[32] N. Shemesh, E. Özarslan, A. Bar-Shir, P.J. Basser, Y. Cohen, Observation of restricted diffusion in the presence of a free diffusion compartment: single- and double-PFG experiments, J. Magn Reson. 200 (2009) 214–225.
[33] M.A. Koch, J. Finsterbusch, Compartment size estimation with double wave vector diffusion-weighted Imaging, Magn. Reson. Med. 60 (2008) 90–101.
[34] T. Weber, C.H. Ziener, T. Kampf, V. Herold, W.R. Bauer, P.M. Jakob, Measurement of apparent cell radii using a multiple wave vector diffusion experiment, Magn. Reson. Med. 61 (2009) 1001–1006.
[35] M.E. Komlosh, E. Özarslan, M.J. Lizak, F. Horkay, V. Schram, N. Shemesh, Y. Cohen, P.J. Basser, Pore diameter mapping using double pulsed-field gradient MRI and its validation using a novel glass capillary array phantom, J. Magn. Reson. 208 (2011) 128–135.
[36] N. Shemesh, T. Adiri, Y. Cohen, Probing microscopic architecture of opaque heterogeneous systems using double-Pulsed-Field-Gradient NMR, J. Am. Chem. Soc. 133 (2011) 6028–6035.
[37] N. Shemesh, Y. Cohen, Microscopic and compartment shape anisotropies in gray and white matter revealed by angular bipolar double-PFG MR, Magn. Reson. Med. 65 (2011) 1216–1227.
[38] J. Finsterbusch, Extension of the double-wave-vector diffusion-weighting experiment to multiple concatenations, J. Magn. Reson. 198 (2009) 174–182.
[39] J. Finsterbusch, Numerical simulations of short-mixing-time double-wave-vector diffusion-weighting experiments with multiple concatenations on whole-body MR systems, J. Magn. Reson. 207 (2010) 274–282.
[40] J. Finsterbusch, M.A. Koch, A tensor approach to double wave vector diffusion-weighting experiments on restricted diffusion, J. Magn. Reson. 195 (2008) 23–32.
[41] M. Lawrenz, M.A. Koch, J. Finsterbusch, A tensor model and measures of microscopic anisotropy for double-wave-vector diffusion-weighting experiments with long mixing times, J. Magn. Reson. 202 (2010) 43–56.
[42] S.N. Jespersen, N. Buhl, The displacement correlation tensor: microstructure, ensemble anisotropy and curving fibers, J. Magn. Reson. 208 (2011) 34–43.
[43] M.A. Koch, J. Finsterbusch, Numerical simulation of double-wave vector experiments investigating diffusion in randomly oriented ellipsoidal pores, Magn. Reson. Med. 62 (2009) 247–254.
[44] M.D. Hurlimann, Effective gradients in porous media due to susceptibility differences, J. Magn. Reson. 131 (1998) 232–240.
[45] P.N. Sen, S. Axelrod, Inhomogeneity in local magnetic field due to susceptibility contrast, J. Appl. Phys. 86 (1999) 4548–4554.
[46] G. Zheng, W.S. Price, Suppression of background gradients in (B-0 gradient-based) NMR diffusion experiments, Concepts Magn. Reson. A 30A (2007) 261–277.
[47] R.M. Cotts, M.J.R. Hoch, T. Sun, J.T. Markert, Pulsed Field Gradient stimulated echo methods for improved NMR diffusion measurements in heterogeneous systems, J. Magn. Reson. 83 (1989) 252–266.
[48] J. Finsterbusch, Generalized MAGSTE with bipolar diffusion-weighting gradient pulses, J. Magn. Reson. 199 (2009) 214–224.
[49] P.Z. Sun, J.G. Seland, D. Cory, Background gradient suppression in pulsed gradient stimulated echo measurements, J. Magn. Reson. 161 (2003) 168–173.
[50] Y.Q. Song, Determining pore sizes using an internal magnetic field, J. Magn. Reson. 143 (2000) 397–401.
[51] L. Avram, Y. Assaf, Y. Cohen, The effect of rotational angle and experimental parameters on the diffraction patterns and micro-structural information obtained from q-space diffusion NMR: implication for diffusion in white matter fibers, J. Magn. Reson. 169 (2004) 30–38.
[52] L. Avram, E. Özarslan, Y. Assaf, A. Bar-Shir, Y. Cohen, P.J. Basser, Three-dimensional water diffusion in impermeable cylindrical tubes: theory versus experiments, NMR Biomed. 21 (2008) 888–898.
[53] A. Bar-Shir, L. Avram, E. Özarslan, P.J. Basser, Y. Cohen, The effect of the diffusion time and pulse gradient duration ratio on the diffraction pattern and the structural information estimated from q-space diffusion MR: experiments and simulations, J. Magn. Reson. 194 (2008) 230–236.
[54] A. Bar-Shir, Y. Cohen, Crossing fibers, diffractions and nonhomogeneous magnetic field: correction of artifacts by bipolar gradient pulses, Magn. Reson. Imaging 26 (2008) 801–808.
[55] J.F. Kuntz, P. Palmas, D. Canet, Diffusive diffraction measurements in porous media: effect of structural disorder and internal magnetic field gradients, J. Magn. Reson. 188 (2007) 322–329.